Noise-Related Shear-Layer Dynamics in Annular Jets

R. W. Wlezien* and V. Kibens†
McDonnell Douglas Corporation, St. Louis, Missouri

Suppression of low-frequency noise has been observed for subsonic annular jets with extended centerbodies. The dynamics of annular jets both with and without centerbody extensions were investigated experimentally to determine the noise-reduction mechanism. For small annular heights, the dynamics of the shear layer are modified by the presence of the centerbody extension and the jet instability mode is effectively suppressed. When the centerbody is truncated at the nozzle exit plane, the flowfield quickly reverts to a form similar to a jet from a round nozzle with equivalent cross-sectional area. Configurations with large annulus heights also generate shear layers with characteristics comparable to a round jet. Detailed spectral contour maps are used to illustrate the spatial development of the velocity spectrum, and the limitations of single-point measurements are discussed.

Introduction

A NOZZLE with an extended porous centerbody was introduced by Maestrello[1,2] primarily as a device for reducing supersonic jet noise. Detailed acoustic measurements for a parametrically varying series of nozzles were obtained by Bauer,[3] and flowfield measurements were conducted by Kibens and Wlezien[4] to determine the noise-suppression mechanism. It was determined that shock-associated noise at supersonic pressure ratios is reduced by attenuation of the core flow shock system. A more detailed description of these results is given in Ref. 5.

Maestrello[2] and Bauer[3] also observed significant sound reduction at subsonic velocities, for which the noise-reduction mechanism clearly must be different. In both investigations far-field microphone correlations were found to have maxima at zero time delay, in contrast to a round jet for which the maxima occur over a wide range of delays. The correlations imply that the sound sources for a jet with an extended centerbody are located over a compact segment of the shear layer. Maestrello[2] attributed the source concentration to a reduction in the length of the potential core. Bauer[3] proposed that the turbulent structure of the jet is modified by the presence of the centerbody and that noise is reduced because vortex pairing is inhibited.

This paper summarizes an investigation of the noise-suppression mechanisms in subsonic annular jets. The role of large-scale turbulence in the generation of jet noise[6-9] and the recent shift of attention to the control of turbulence as a basis for noise reduction provide motivation to link flow characteristics to the acoustic far field. The acoustic results presented in detail in Ref. 5 are summarized briefly here. In this paper the authors focus on the shear-layer dynamics of annular jets. The degree to which the shear layer is modified by the presence of a centerbody is measured, and it is determined whether the modifications are consistent with the observed noise reduction. Hot-wire spectra, mean-flow distributions, and a novel spectral mapping technique are used to document the dynamic characteristics of flows having a variety of centerbody geometries.

Received Dec. 14, 1983; revision received June 11, 1984.

*Senior Scientist, McDonnell Douglas Research Laboratories. Member AIAA.

†Principal Scientist, McDonnell Douglas Research Laboratories. Associate Fellow AIAA.

Experimental Apparatus and Approach

An annular nozzle with an extended centerbody is illustrated schematically in Fig. 1. D is the nominal diameter of the nozzle exit and h the height of the annulus between the nozzle lip and centerbody. L denotes the length of the centerbody downstream of the nozzle exit plane. The radial and axial coordinates originate on the system centerline and at the exit plane of the nozzle, respectively.

Centerbody models were installed in McDonnell Douglas Research Laboratories (MDRL) Aerodynamic Noise Facility flow system to obtain flowfield data under more controlled conditions than those in the acoustic tests. The flow system is essentially that described by Kibens,[10] with an electronically controlled blower and a muffler to produce a stable and quiet flow source. A low-angle conical diffuser is followed by a settling chamber with honeycomb and screens, and a bicubic contraction having a 23:1 area ratio which increases with the addition of centerbodies.

The centerbodies used for these tests had a solid surface with the same shape downstream of the jet exit plane as the models in Ref. 5. A blunt nose extended into the contraction (Fig. 1) to prevent flow separation by providing a smooth variation of cross-sectional area. The centerbodies were suspended by three fine stainless-steel wires at both the upstream and downstream ends to eliminate flow interference. The wires were held sufficiently taut to prevent centerbody vibration and were adjusted to maintain concentricity between the centerbody and the nozzle. The extended centerbody configurations are denoted SC-series (solid centerbody) in Table 1 and have annular heights of 0.1 and 0.25 diameter. Configuration SC10 is shown in Fig. 2a. A reference annular jet without an extended centerbody (configuration AJ) was obtained by truncating the centerbody at the nozzle exit plane and supporting it with a 3-mm-diam rod (Fig. 2b). Configuration RJ consisted of the same basic nozzle without a centerbody.

Hot-wire measurements of the axial velocity component were obtained using a Thermo Systems Model 1050 anemometer. An analog polynomial linearizer was used to linearize the velocity signal; spectra of the linearized velocity were computed by an HP3582A real-time spectrum analyzer. The instrumentation and data acquisition were controlled in real-time by a DEC PDP 11/70 data acquisition system. Flow velocity was monitored by the system to ensure stable and repeatable test conditions. A computer-controlled, three-degree-of-freedom traversing system was used to position hot-wire sensors in the flowfield. Mean and rms velocities were computed by directly digitizing the hot-wire signal and linearizing it with a fourth-order polynomial. The sensors were recalibrated under computer control prior to each run to compensate for drift and temperature variation.

Results and Discussion

One-third-octave sound-reduction spectra for a series of nozzles with porous centerbodies are shown in Fig. 3. The spectra are based on the meaurements of Bauer et al.[5] at an exit velocity $U_0 = 278$ m/s. All nozzles had the same nominal exit area as a $D = 118$-mm reference nozzle, and force measurements indicated that all nozzles produced thrust within 7% of the reference. The far-field noise measurements were obtained in an anechoic chamber using a microphone at 30 deg from the jet axis. The noise-reduction spectra are given in decibels relative to the noise spectrum for the reference jet.

Figure 3c indicates that a short centerbody with a large annular height produces a noise reduction of 1-2 dB over a wide frequency range. Noise-reduction spectra for nozzles with the same $0.235D$ annular height (Fig. 3b) show that increasing the centerbody length by approximately 3 diameters dramatically increases the noise reduction near $St = 0.2$. The low-frequency noise suppression is further augmented by increasing the centerbody length to $4.45D$. In Fig. 3a, the noise-suppression spectra for a smaller annular height indicate that there is as much as a 9-dB noise reduction near $St = 0.2$ for a length of 5.15 diameters, and approximately 7 dB for a shorter centerbody. The surface porosity, which is important at supersonic velocities, has virtually no effect at subsonic conditions.

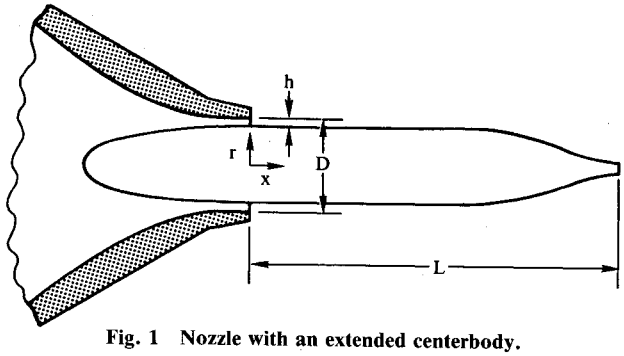

Fig. 1 Nozzle with an extended centerbody.

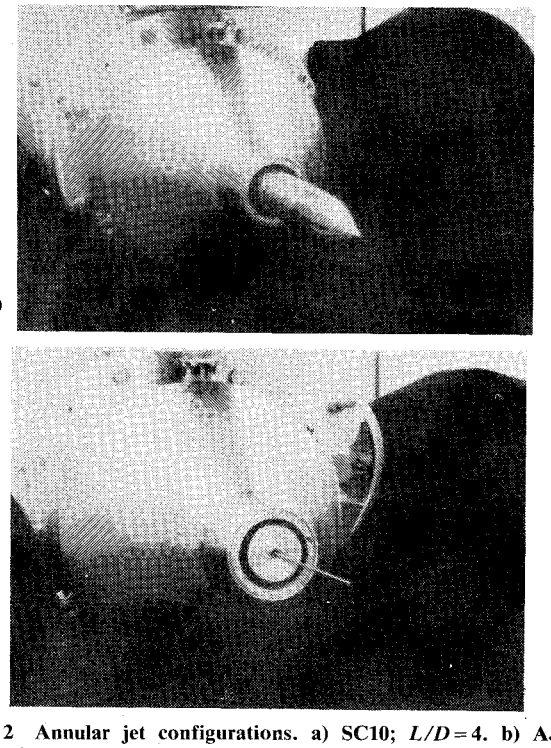

a)

Fig. 2 Annular jet configurations. a) SC10; $L/D = 4$. b) AJ10; $L/D = 0$.

Table 1 Nozzle geometric parameters

Configuration[a]	h/D[b]	L/D
RJ	0	0
AJ10	0.1	0
SC10	0.1	4.0
SC25	0.25	3.3

[a] RJ = round jet; AJ = annular jet without centerbody extension; SC = annular jet with solid centerbody extension. [b] $D = 63.5$ mm.

The acoustic results imply that the geometry of the centerbody modifies the characteristics of the shear layer in such a way as to reduce the generated noise. The fact that the maximum noise reduction occurs near $St = 0.2$ strongly suggests that the jet instability mode (the mode that occurs at the end of the potential core[7]) is suppressed. Because of the apparent unimportance of surface porosity, solid-surface models were used for the detailed flow measurements.

The dynamics of shear-layer development were investigated by spectral analysis of data from hot-wire sensors located within or near the shear layer. Surveys of the shear-layer-instability frequencies were conducted for a baseline round jet (RJ) and solid centerbody configurations with two annular heights (SC10 and SC25). The boundary between the core flow and the shear layer was chosen as the optimal sensor path, since at this location the signal-to-noise ratio between the periodic motion and the background turbulence is greatest. For the round jet, the inner edge of the potential core was tracked until the jet centerline was reached, and the probe was located on the jet centerline farther downstream. In an annular jet, the potential core terminates much closer to the nozzle exit plane than in a round jet. When the potential core terminated before the end of the centerbody, the sensor was moved along the outer edge of the centerbody boundary layer and along the jet centerline beyond the end of the centerbody.

Figure 4 illustrates the streamwise development of the shear-layer Strouhal number for $U_0 = 21$ m/s. The data for the large-annulus jet (SC25) and the round jet (RJ) in Fig. 4a follow virtually the same trend with increasing streamwise distance. Measurements in both flows exhibit a double frequency characteristic of the initial shear-layer instability, f_s. This effect is a consequence of the presence of the hot-film sensor; a smaller hot-wire probe having minimal flow interference was

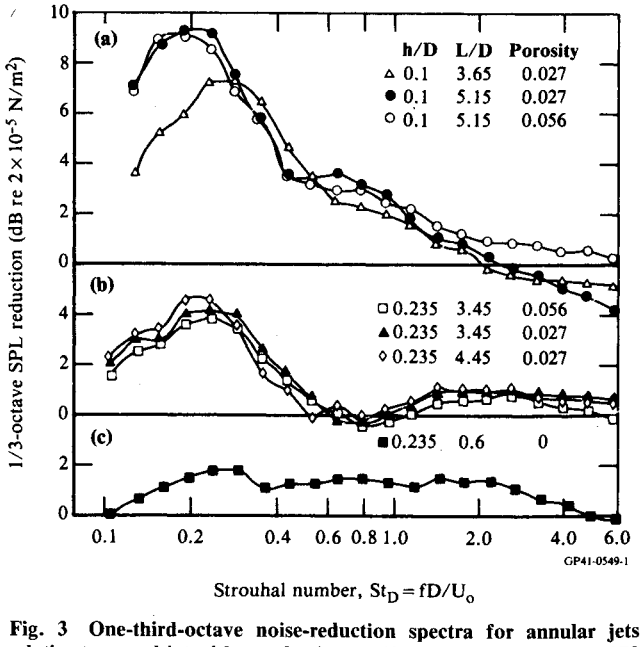

Fig. 3 One-third-octave noise-reduction spectra for annular jets relative to round jet with equal exit area (data from Ref. 5); $U_0 = 278$ m/s.

used for measurements presented later in this paper, and the spurious frequency was eliminated. The formation of at least two subharmonic frequencies, $f_s/2$ and $f_s/4$, is evident in Fig. 4a; a third pairing to form $f_s/8$ is suggested. For x/D beyond 2.5, the Strouhal number appears to be independent of previous shear-layer frequencies and is approximately equal to 0.4. In a round jet, the appearance of an instability frequency independent of the initial shear-layer frequencies is taken as evidence of the jet mode (see Ref. 7). The appearance of this frequency for the SC25 configuration indicates that the centerbody has little influence on the jet dynamics for $h/D=0.25$ or more.

In Fig. 4b the data for the SC10 nozzle exhibit a similar trend for $x/D<1$. The initial shear-layer frequency and evidence of two subsequent pairings can be seen. Although the exit velocity is the same as in Fig. 4a, the initial instability frequency and its subharmonics are approximately 25% higher, the significance of which is discussed below. For $x/D>1$, the spectral development of the SC10 jet differs from that of the other configurations. There is no indication of the third subharmonic or the jet column modes, and the peak Strouhal number decreases rapidly with streamwise distance. At $x/D=5$, a Strouhal number of 0.1 is observed for configuration SC10 in comparison with 0.4 for configurations RJ and SC25.

The initial shear-layer-velocity profiles and momentum thicknesses for configuration SC10 were measured to clarify the observed increase in the instability frequency. Figure 5 shows that the Strouhal number based on momentum thickness has an approximately constant value of 0.016, which is consistent with the analysis of Michalke[11] for round jets with thin shear layers. This result implies that the shear layer becomes unstable at a higher frequency because the initial shear layer is thinner. The momentum thickness of the shear layer is inversely proportional to the nozzle contraction ratio, and the large-diameter centerbody increases the ratio to approximately 64:1.

It is apparent that the presence of the large extended centerbody modifies the development of the shear layer and that, in particular, it interferes with the formation of the jet mode. This effect is further illustrated in Fig. 6, in which the velocity spectra are compared for the three nozzle configurations at $x/D=1.6$. The RJ and SC25 spectra have similar energy distributions, but the energy in the peak is suppressed for configuration SC10. Again, the small-diameter centerbody has little influence on the formation of long-wavelength instabilities. When the annular height is small, the length of the annular potential core is significantly reduced and the jet shear layer exhausts the region available for growth before the jet scales can develop.

A question that immediately arises is whether a purely annular nozzle configuration or an annular jet with an added centerbody extension is responsible for the flowfield modification. Direct comparisons between turbulence-intensity levels in the annular and round jets can be misleading as the overall mass and momentum flux differ for the two jets, even though the outer nozzle diameters are the same. An annular jet (configuration AJ10) having the same exit plane geometry as the solid-centerbody nozzle but with no centerbody extension beyond the exit plane was chosen as a reference configuration for the detailed turbulence-intensity measurements. This reference case permits a direct evaluation of the influence of the extended centerbody on the developing shear layers.

Contour plots of the mean velocity and longitudinal turbulence-intensity distributions for configurations SC10 and AJ10 are presented in Fig. 7. Although the exit area and velocity of the two flows are identical, the velocity distributions show considerable differences in mean velocity and turbulence intensity. In Figs. 7a and 7c, increasing gray levels represent increasing U/U_0, with an interval of 0.11 between contours. The streamwise growth of the jet is illustrated by the path of the lowest contour level, $U/U_0=0.11$. The outer boundary of the SC10 jet initially grows more rapidly than that of the AJ10 jet, but by $x/D=8$ the radial location of all the contour lines indicates that the mean velocity profiles are virtually the same for both jets. For the AJ10 configuration, the core flow and shear layers deflect toward the jet centerline for $x/D<1$. The separated zone behind the truncated centerbody closes by $x/D=3$, beyond which the flow develops similarly to a round jet with an equivalent exit area. A comparison of the turbulence intensity distributions suggests that most of the turbulent mixing occurs for $x/D<3$ when the centerbody is extended (Fig. 7b), whereas turbulence levels remain high until $x/D=6$ for the truncated centerbody configuration (Fig. 7d).

The mean-velocity and turbulence-intensity measurements are limited in that they do not include the transfer of energy among turbulent scales. Single-point velocity spectra show the

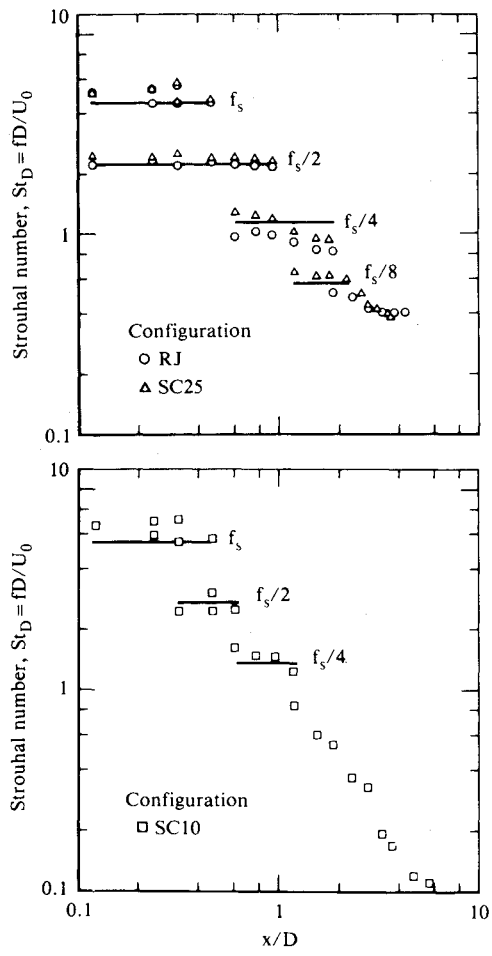

Fig. 4 Axial development of shear-layer frequencies for round and annular jets; $U_0=21$ m/s.

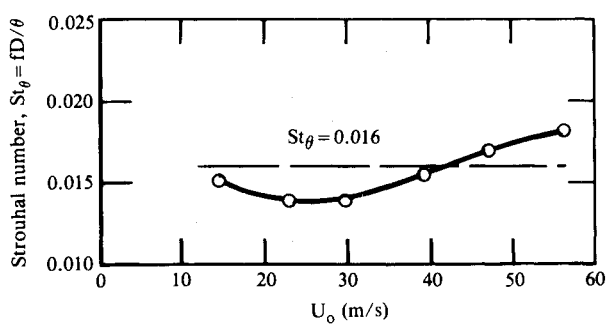

Fig. 5 Variation of initial shear-layer instability St_θ with velocity; configuration SC10, $x/D=0.02$.

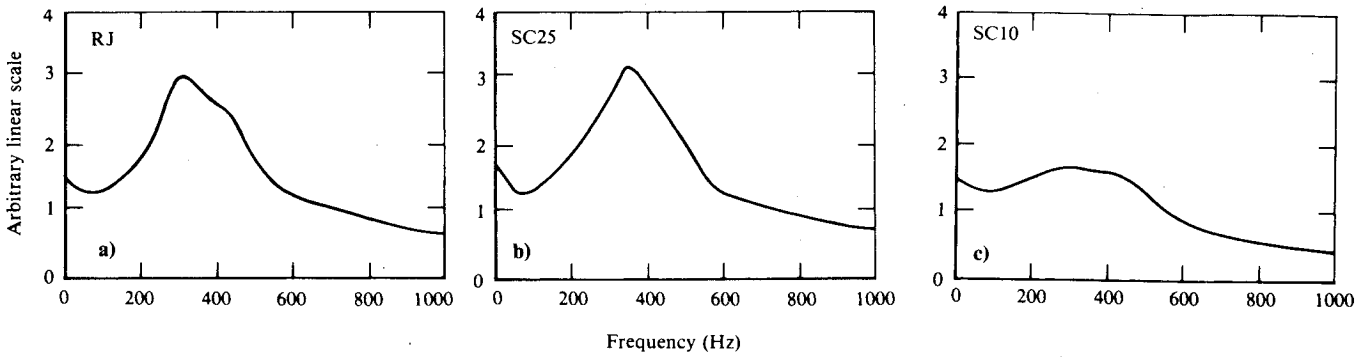

Fig. 6 Comparison of round and annular jet velocity spectra; $x/D = 1.6$, $U_0 = 21$ m/s.

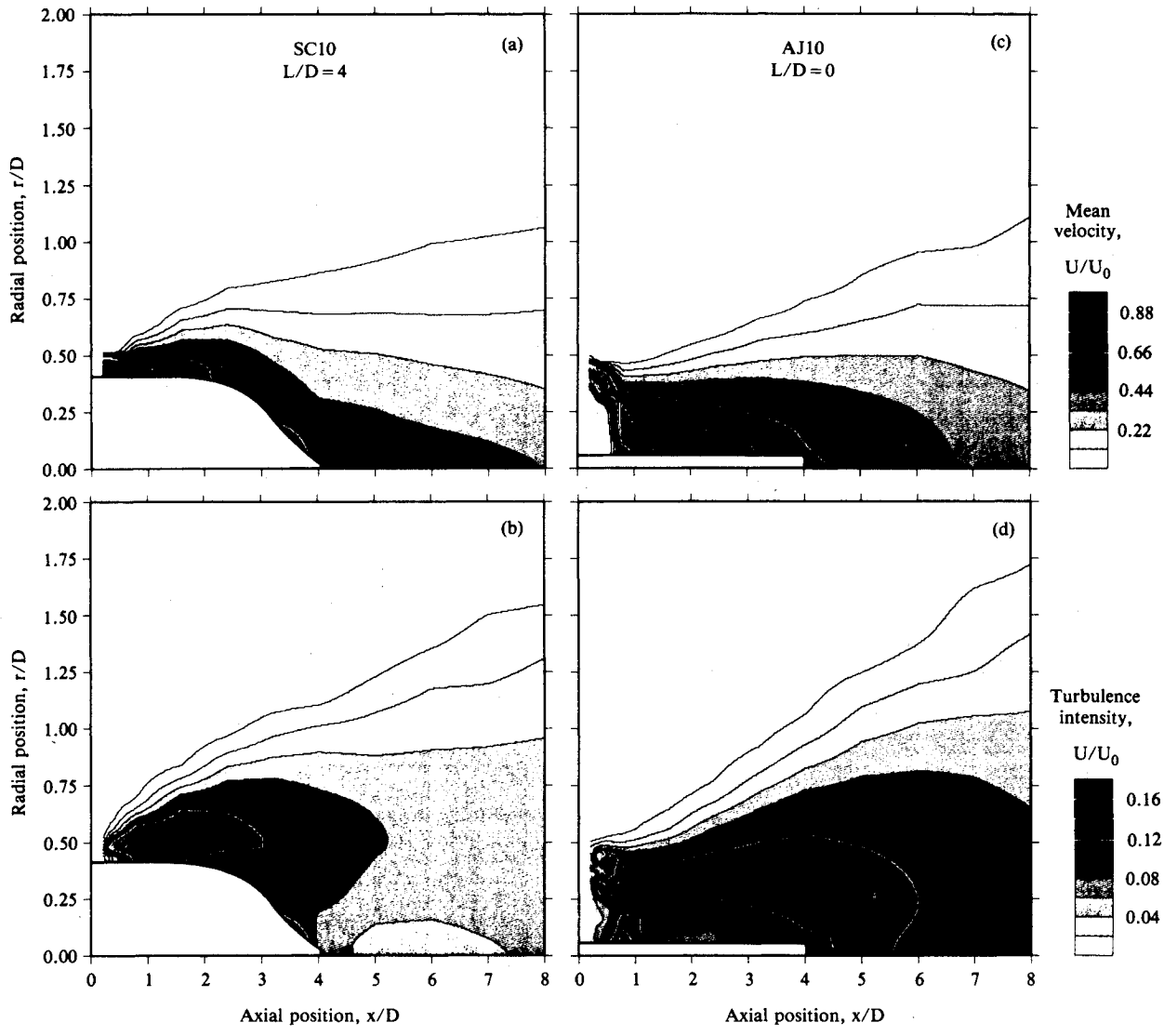

Fig. 7 Distribution of mean velocity and turbulence intensity for annular jets; $U_0 = 30$ m/s.

energy distribution among scales but are not sufficiently global to adequately represent complex flowfields. A more comprehensive description of the jet dynamics can be achieved by mapping turbulent-energy distributions in both wave number and physical space. Measurement of the full three-dimensional spectra is beyond the scope of this experiment; a more tractable subset has been implemented here. A one-twelfth-octave spectral mapping technique has been developed in which the longitudinal-velocity-fluctuation spectra are displayed in a contour map as a function of a single spatial coordinate.

Fractional-octave spectra facilitate the description of shear-layer instabilities in a number of ways. A logarithmic frequency representation is useful because the shear-layer instability progresses to scales of increasing size through vortex pairing, and frequencies are successively halved. A direct logarithmic frequency plot is misleading because the area under the low-frequency portion of the curve disproportionately

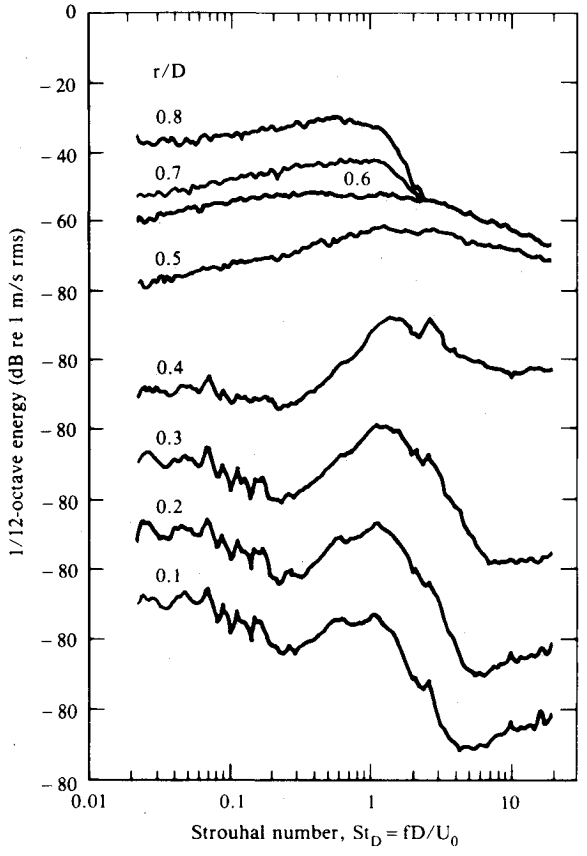

Fig. 8 Variation of one-twelfth-octave velocity spectra across round jet; $U_0 = 30$ m/s, $x/D = 0.8$.

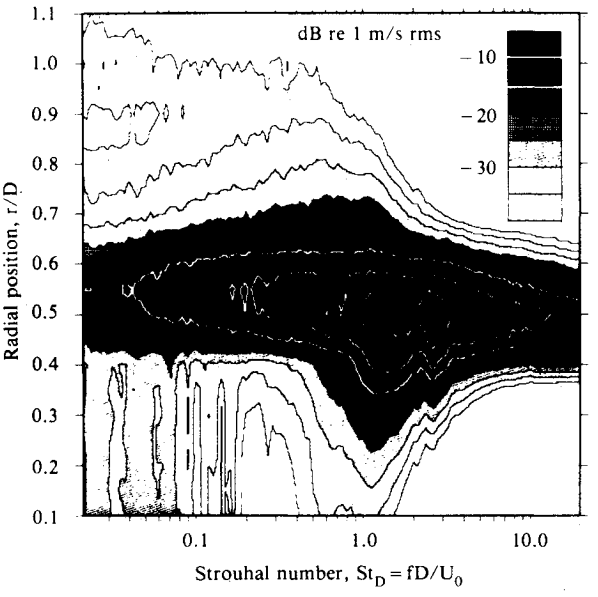

Fig. 9 One-twelfth-octave spectral map of round-jet shear layer; $U_0 = 30$ m/s, $x/D = 0.8$.

weights that part of the spectrum; this difficulty can be alleviated by increasing the effective filter bandwidth linearly with frequency. One-third-octave filters are customarily used for acoustic spectra; increased resolution, one-twelfth-octave filters were implemented for this study.

The curve labeled 0.4 in Fig. 8 is a typical spectrum for a single point in the shear layer of a round jet. The fluctuating velocity intensity in each frequency band is expressed in decibels relative to 1 m/s rms. There is a broad peak centered about $St = 1.5$ and a sharper peak with less total energy approximately at $St = 2.6$. The sharp peak is a vestige of the first pairing of the shear-layer vortices and corresponds to $f_s/2$. When a series of spectra from various radial locations are plotted together (Fig. 8), the spatial variation of the turbulence spectra is apparent. The sharp peak becomes less pronounced away from the center of the shear layer. In the core flow region, there is evidence of energy at the subharmonic of this peak. The broad peak also changes with radial position, but it is difficult to assess the variation of fluctuation intensity and peak Strouhal number from this data format.

Figure 9 displays the same spectral data in the form of isointensity contours as a function of Strouhal number and radial position, with gray levels representing the log of the axial turbulence intensity. It is apparent that the most energetic portion of the flow is in the center of the jet shear layer, $r/D = 0.5$. The intensity level in the sharp peak near $St = 2.6$ drops off much more quickly with distance from the center of the shear layer than that in the dominant wide peak. The Strouhal number corresponding to the center of the peak decreases with distance from the center of the shear layer. The portion of the spectral map having significant intensity at high frequencies indicates that the shear layer extends from $r/D = 0.3$ to 0.7. The low-frequency fluctuations outside the shear layer are induced by the large vortices within the layer. The frequency of peak fluctuation intensity decreases with distance from the center of the shear layer, presumably because the largest vortices generate the strongest induced field. A comparison of Figs. 8 and 9 demonstrate that the spectral map presents a detailed and more useful description of the turbulent energy than a collection of individual spectra.

A sequence of spectral maps taken at various streamwise locations for the annular and extended centerbody configurations are compared in Fig. 10. During the initial stage of shear-layer development, there is considerable similarity between the two flows (Figs. 10a-f). At $x/D = 0.2$, in Figs. 10a and 10d, the nozzle lip shear layers at $r/D = 0.5$ develop a primary instability, f_{s_o}, near a Strouhal number of 7. The annular configuration also has an inner shear layer at $r/D = 0.4$, which develops an instability frequency, f_{s_i}, near $St = 10$. The instability frequency of the inner layer, f_{s_i}, is higher than that of the outer layer, f_{s_o}, because the boundary layer follows a shorter development path over the nose of the centerbody, and consequently produces a thinner shear layer. The annular configuration also has significant energy at $St = 0.2$ for sensor locations behind the truncated centerbody (Fig. 10a, $r/D \leq 0.35$; Fig. 10b, $r/D \leq 0.3$; Fig. 10c, $r/D \leq 0.25$), which indicates that the recirculation zone serves as a feedback path for low-frequency perturbations that occur further downstream.

The progression of the jet instability to decreasing Strouhal numbers can be observed by following the sequence of extended centerbody maps (SC10) from $x/D = 0.2$ to 6.4 (Figs. 10d-f, 10j-l). The spectral peak, the darkest region of the map, broadens in both Strouhal number and radial extent and moves to lower Strouhal numbers with increasing x/D. At a fixed axial location, the Strouhal number of the peak decreases with distance from the jet centerline, as shown in Fig. 10f. In general, similar trends are observed for all configurations, including round and coannular jets, for which spectral maps have been generated. The strong spatial dependence of the turbulent-energy spectral distribution implies that single-point characterizations of the jet instability modes can be misleading. At a fixed point in the jet, distinct spectral peaks are evident, but the Strouhal number of the peak can vary greatly with sensor position. Such variability can explain, in part, the wide range of jet column Strouhal numbers reported in the literature.

The formation of subharmonic frequencies through pairings is clearly shown in Figs. 10d and 10e for configuration SC10. At $r/D = 0.5$ peaks develop near Strouhal numbers of 3.5 and 1.75, although the peaks broaden with increasing x/D and decreasing Strouhal number because of jitter in the pair-

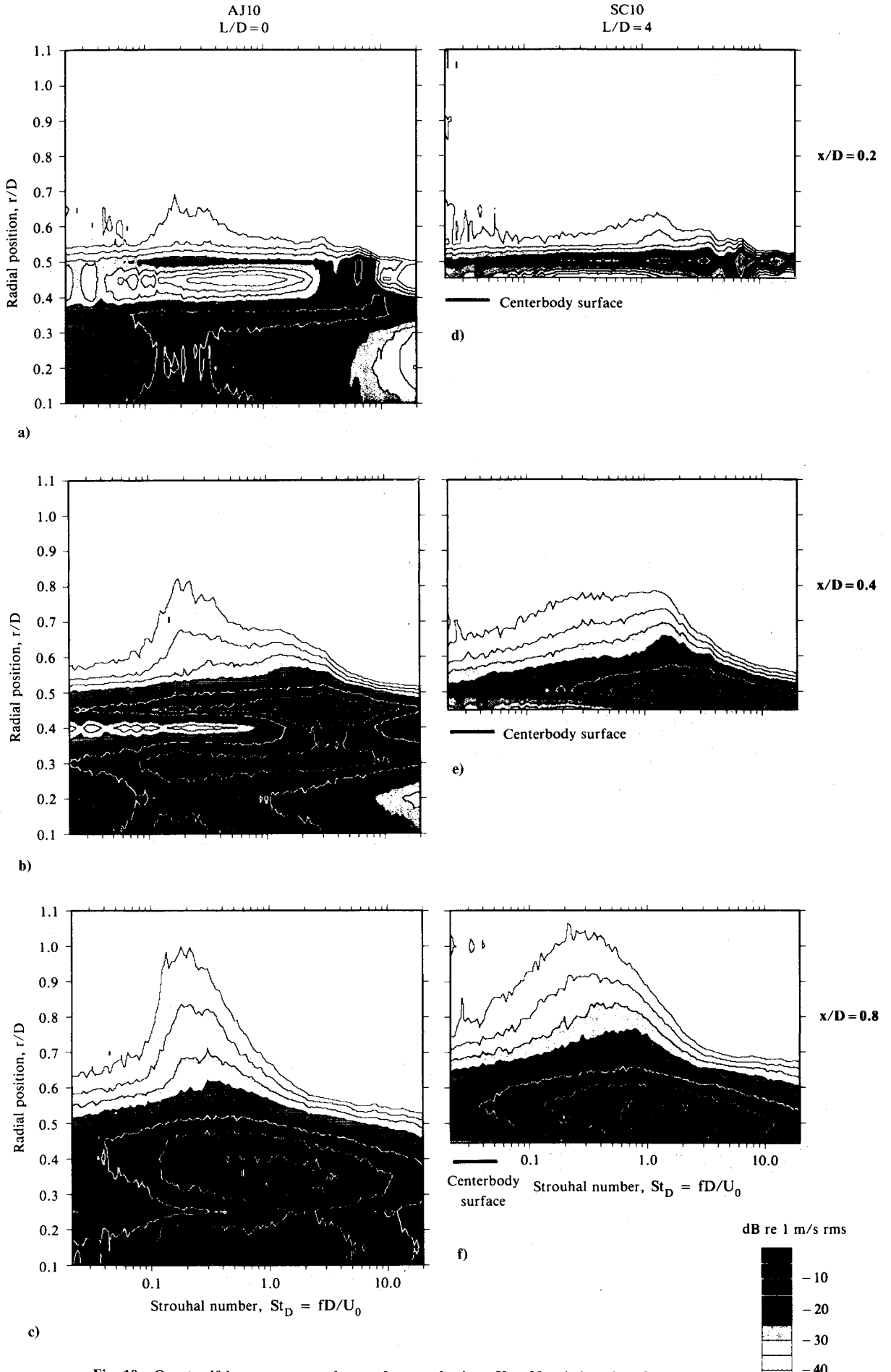

Fig. 10 One-twelfth-octave spectral maps for annular jets; $U_0 = 30$ m/s (continued on next page).

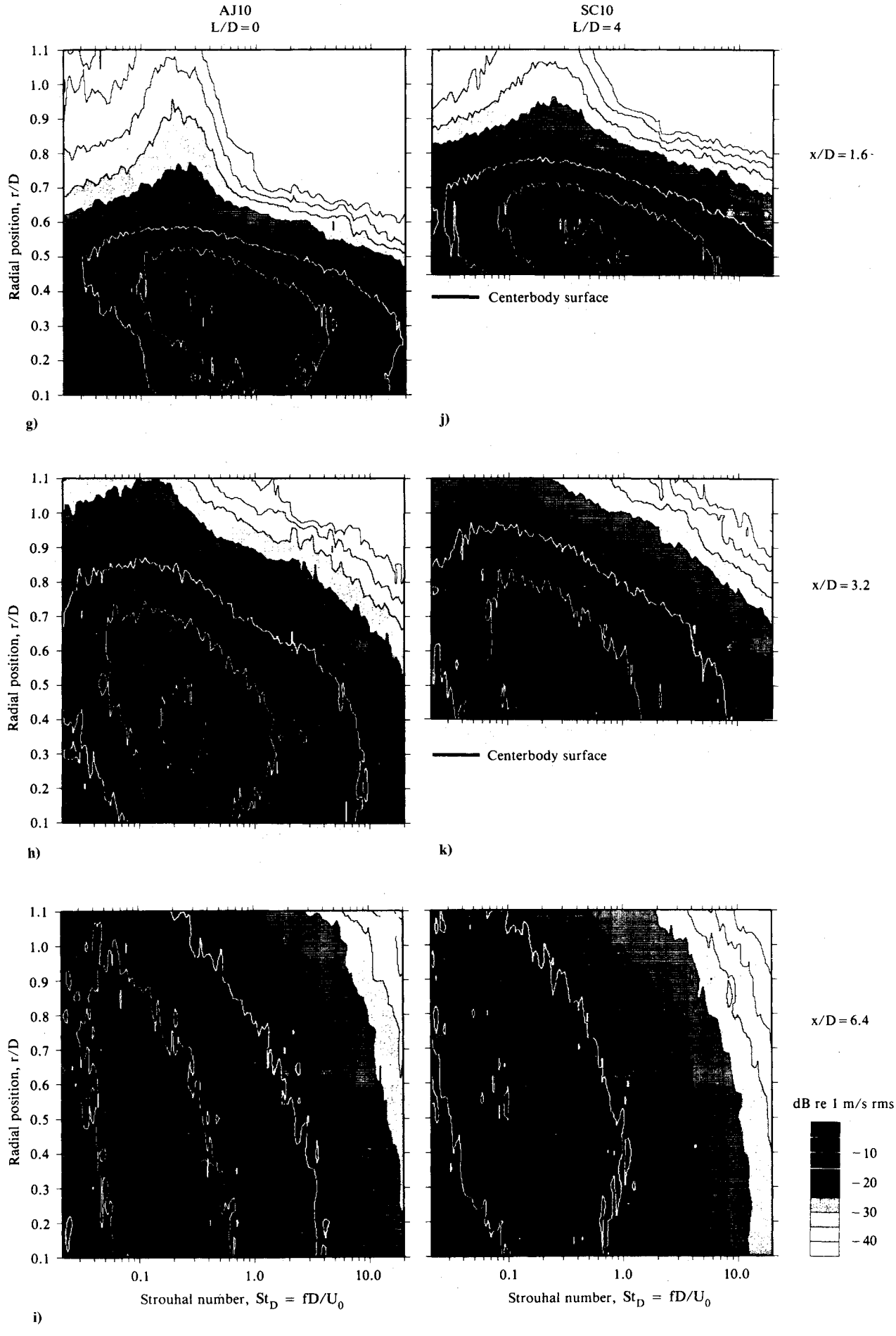

Fig. 10 Concluded.

ing locations. By $x/D=0.8$, the instability peak is almost two octaves wide. Subharmonics in the outer shear layer for configuration AJ10 appear at $r/D=0.45$ in Fig. 10b, although the second subharmonic frequency is not as energetic as that for configuration SC10. Any evidence of pairing in the inner shear layer (Fig. 10a, $r/D=0.35$; Fig. 10b, $r/D=0.3$) is observed by the unsteadiness inside the recirculating separated region.

The outer shear layer of the annular jet moves toward the jet centerline with increasing x/D, as observed in the mean-flow data. The spectral-energy distributions in the outer shear layer remain nearly identical through $x/D=0.8$ when the displacement of the shear layer is taken into consideration. For example, at $x/D=0.8$, the spectral map for configuration AJ10 in Fig. 10c is similar to that for configuration SC10 in Fig. 10f when it is shifted upward by 0.15 diameter.

Beyond $x/D=1.6$, the instability characteristics of the two flows diverge. At $x/D=1.6$, the extended centerbody flow exhibits an energy peak near the surface of the centerbody and centered at $St=0.6$ (Fig. 10j), whereas the annular jet (Fig. 10g) has less energy at the same location. At $x/D=3.2$ and 6.4, the extended centerbody flow (Figs. 10k and 10l) produces turbulent-energy peaks that are significantly weaker than those for the annular flow (Figs. 10h and 10i). The difference constitutes a large influence on the flow by the extended centerbody. Intense turbulent mixing occurs earlier in the flow development when the centerbody is present, thereby producing lower turbulence levels downstream. Intense activity occurs farther downstream in the annular jet, where the Strouhal number is lower and turbulence scales are larger.

Conclusions

The primary conclusion of this investigation is that an annular nozzle with an extended centerbody interferes with the formation of the jet instability mode and suppresses jet noise. The noise-suppression spectra show that the greatest noise reduction is in the vicinity of $St=0.2$, the same frequency band for which turbulent fluctuation intensities are suppressed by the extended centerbody. The following trends are observed in both acoustic and flow measurements.

1) An annular jet with a short or truncated centerbody produces negligible modification to either the noise or velocity spectra in comparison with a reference round jet. The velocity distribution for an annular jet without a centerbody extension quickly reverts to a mean profile similar to that of a round jet. Turbulence intensity is high for $3\leq x/D\leq 6$ where the jet instability occurs.

2) A small-annular-height nozzle with a long centerbody produces the greatest noise suppression. The reduction is primarily at the low frequencies for which turbulence reduction is also observed. The initial-shear-layer modes exist as in the round jet, but the shortened annular potential core limits the axial domain over which the shear layer can experience unconstrained growth.

3) A jet from a nozzle with a large annular height produces moderate low-frequency noise reduction, although negligible modification to the velocity spectra is observed.

4) An extended centerbody causes energy to be channeled into the shear-layer instabilities near the exit of the nozzle where the scales are small. The flow is more competely mixed by the time it reaches an axial location where the jet mode forms, thereby reducing the energy available for long-wavelength instabilities. This observation is consistent with the far-field correlations of Maestrello[2] and Bauer[3] that show the sound source to be concentrated near the jet origin.

Finally, the utility of a global approach to flowfield turbulent spectra has been demonstrated with the spectral mapping technique. The maps are a spatial analog of a voiceprint and present a detailed picture of the development of shear-layer instabilities. The limitations and inconsistencies of single-point measurements are clarified and may help to explain the wide range of jet-mode Strouhal numbers observed among various facilities.

Acknowledgment

This research was conducted under the McDonnell Douglas Independent Research and Development program.

References

[1]Maestrello, L., "Initial Results of a Porous Plug Nozzle for Supersonic Noise Suppression," NASA TM-78802, 1978.

[2]Maestrello, L., "An Experimental Study on Porous Plug Jet Noise Suppressors," AIAA Paper 79-0673, 1979.

[3]Bauer, A. B., "Jet Noise Suppression by Porous Plug Nozzles," AIAA Paper 81-1993, 1981.

[4]Kibens, V. and Wlezien, R. W., "Porous-Plug Flowfield Mechanisms for Reducing Supersonic Jet Noise," AIAA Paper 83-0774, 1983.

[5]Bauer, A. B., Kibens, V., and Wlezien, R. W., "Jet Noise Suppression by Porous Plug Nozzles," NASA CR-3613, 1982.

[6]Ffowcs-Williams, J. E. and Kempton, A. J., "The Noise from the Large-Scale Structure of a Jet," *Journal of Fluid Mechanics*, Vol. 84, Pt. 4, 1978, pp. 673-694.

[7]Kibens, V., "Discrete Noise Spectrum Generated by an Acoustically Excited Jet," *AIAA Journal*, Vol. 18, April 1979, pp. 434-441.

[8]Moore, C. J., "The Role of Shear-Layer Instability Waves in Jet Exhaust Noise," *Journal of Fluid Mechanics*, Vol. 80, Pt. 2, 1977, pp. 321-367.

[9]Laufer, J. and Yen, T. C., "Noise Generation by a Low Mach Number Jet," *Journal of Fluid Mechanics*, Vol. 134, 1983, pp. 1-31.

[10]Kibens, V., "Interaction of Jet Flowfield Instabilities with Flow System Resonances," AIAA Paper 80-0963, 1980.

[11]Michalke, A., "The Instability of a Compressible Circular Jet with Finite Boundary Layer Thickness," *Zeitschrift für Flugwissenschaften*, Vol. 19, No. 8/9, 1971, pp. 319-328 (in German).